nature photonics

LETTERS

https://doi.org/10.1038/s41566-018-0216-2

Efficient light generation from enhanced inelastic electron tunnelling

Haoliang Qian[1,5], Su-Wen Hsu[2,5], Kargal Gurunatha[2], Conor T. Riley[2], Jie Zhao[1], Dylan Lu[1], Andrea R. Tao[2,3]* and Zhaowei Liu[1,3,4]*

Light emission from biased tunnel junctions has recently gained much attention owing to its unique potential to create ultracompact optical sources with terahertz modulation bandwidth[1–5]. The emission originates from an inelastic electron tunnelling process in which electronic energy is transferred to surface plasmon polaritons and subsequently converted to radiation photons by an optical antenna. Because most of the electrons tunnel elastically, the emission efficiency is typically about 10^{-5}–10^{-4}. Here, we demonstrate efficient light generation from enhanced inelastic tunnelling using nanocrystals assembled into metal–insulator–metal junctions. The colour of the emitted light is determined by the optical antenna and thus can be tuned by the geometry of the junction structures. The efficiency of far-field free-space light generation reaches ~2%, showing an improvement of two orders of magnitude over previous work[3,4]. This brings on-chip ultrafast and ultracompact light sources one step closer to reality.

Electrons can tunnel through a metal–insulator–metal (MIM) junction either elastically or inelastically. For elastic tunnelling, electrons tunnel across the barrier layer without energy loss[6]. However, the inelastic tunnelling process may create either phonons or photons as the electrons lose part of their energy in the gap and transition to a lower energy state in the metal counter-electrode. This process can be enhanced in the presence of surface plasmon polaritons around the MIM junction, as first discovered in 1976[1]. Later theoretical[2] and experimental[7–10] studies increased the appeal of the MIM junction because of its ultra-small footprint and ultra-large modulation bandwidth. However, the main challenge for light generation from inelastic electron tunnelling is its low external quantum efficiency (EQE), a production of internal quantum efficiency (IQE) and radiation efficiency. Generally, the IQE describes the efficiency of the inelastic tunnelling event and can be increased by designing a plasmonic structure with a large local density of optical states (LDOS)[7,11,12], and the radiation efficiency can be improved by introducing a high-quality optical antenna[13,14]. Recently, light emission from electrically driven optical antennas made by amorphous (polycrystalline) plasmonic material has been demonstrated[3,4] with quantum efficiencies up to 10^{-4}. Compared with amorphous or polycrystalline plasmonic material, single-crystalline material has lower plasmonic loss[15], which can further enhance the performance of the inelastic tunnel junction. Here, we use single-crystalline silver (Ag) nanocrystals to form tunnel junctions with gap distances of ~1.5 nm. Through geometrical engineering of the junctions to optimize the LDOS and radiation efficiency, we obtain a far-field light emission efficiency up to ~2% at near-infrared frequencies, showing over two orders of magnitude improvement over previous reports[3,4]. The performance is attributed to the very high LDOS obtained by using high-quality atomic-level plasmonic cavities created within the ultra-small gap between two well-faceted Ag nanocrystals, combined with high radiation efficiency achieved by using the edge-to-edge configuration as an optical nanoantenna.

The inelastic tunnelling device is schematically illustrated in Fig. 1a, where photons are emitted from an electronically biased junction formed by two Ag nanocrystals. The nanojunctions are assembled and oriented through a previously reported process of polymer-mediated nanoparticle assembly[16]. The gap distance in the tunnel junction can be precisely controlled by the length of grafted polymers on the cuboid surfaces (Supplementary Section 1). The transmission electron microscope (TEM) image in Fig. 1b confirms that the gap of the tunnel junction is approximately 1.5 nm. High-resolution TEM (HRTEM) in Fig. 1c confirms that the Ag structure is single-crystalline, which is critical to form a high-quality junction and optical antenna.

The total light emission is proportional to the IQE and radiation efficiency[4]. The former is described by Fermi's golden rule which is related to the applied bias voltage and the LDOS. The LDOS ρ can be obtained[4] from $\rho = \rho_0 \times (P_{tot} / P_0)$, where ρ_0 is the vacuum density of states (DOS), P_{tot} is the total dissipated power, and P_0 is the radiated power of a dipole of equal dipole moment in a vacuum environment. The radiation efficiency is typically deduced by calculating the ratio between the radiated power and the total power. The plasmonic mode within an ultra-small tunnelling gap, smoothed at the atomic level, produces an ultra-strong plasmonic field, causing greatly enhanced coupling strength between the two electronic states (φ_1 and φ_2 marked in the inset of Fig. 1a), which can greatly increase the IQE. By engineering the geometry of the nanojunction with different heights (c) of Ag square prisms and different in-plane aspect ratios (b/a) of Ag nanobars, the overall efficiency can be tuned and optimized at a desired range of working frequency.

Figure 2a shows the simulated LDOS and radiation efficiency obtained by placing different dipole polarizations in the centre of the gap, where one can see that x polarization dominates the LDOS and radiation efficiency. The maximum LDOS and radiation efficiency are 3.1×10^5 (in units of the DOS of vacuum) and 24.6%, respectively, for the x polarization. The distribution of the plasmonic resonance field shows that it is concentrated within the gap and overlaps with the junction very well (Supplementary Section 2), promoting the inelastic tunnelling process because of the

[1]Department of Electrical and Computer Engineering, University of California, San Diego, La Jolla, CA, USA. [2]Department of NanoEngineering, University of California, San Diego, La Jolla, CA, USA. [3]Material Science and Engineering, University of California, San Diego, La Jolla, CA, USA. [4]Center for Memory and Recording Research, University of California, San Diego, La Jolla, CA, USA. [5]These authors contributed equally: Haoliang Qian, Su-Wen Hsu.
*e-mail: atao@ucsd.edu; zhaowei@ucsd.edu

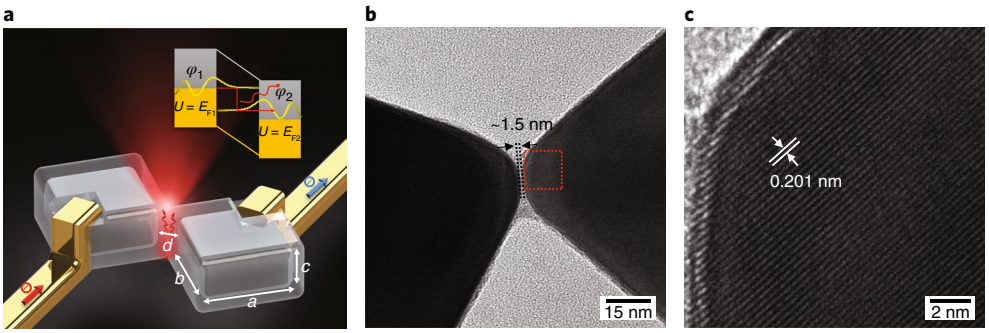

Fig. 1 | Light emission from an electrically driven optical antenna engineered at the atomic level. a, Schematic diagram of the tunnel junction formed by two edge-to-edge Ag single-crystal cuboids encapsulated by a layer of polymer. Here the grafted polymer (polyvinylpyrrolidone) acts as an insulating barrier, as its bandgap is more than 4.7 eV (ref. [27]). The top inset shows that the photons are generated through inelastic electron tunnelling. Here, E_{F1} and E_{F2} are the Fermi energies of the left and right Ag cubes, respectively. The device performance can be engineered by tuning the geometrical parameters of the tunnel junction including the gap size *d*, the size of the cuboids (*a*, *b*, *c*) and the curvature of the Ag cuboid edges. **b**, TEM image of the tunnel junction, where the gap is around 1.5 nm. **c**, Single-crystal lattice of the Ag facet near the tunnel junction (red dashed square in **b**), imaged by high-resolution TEM. The lattice distance is about 0.201 nm, which corresponds to the Ag {200} lattice spacing.

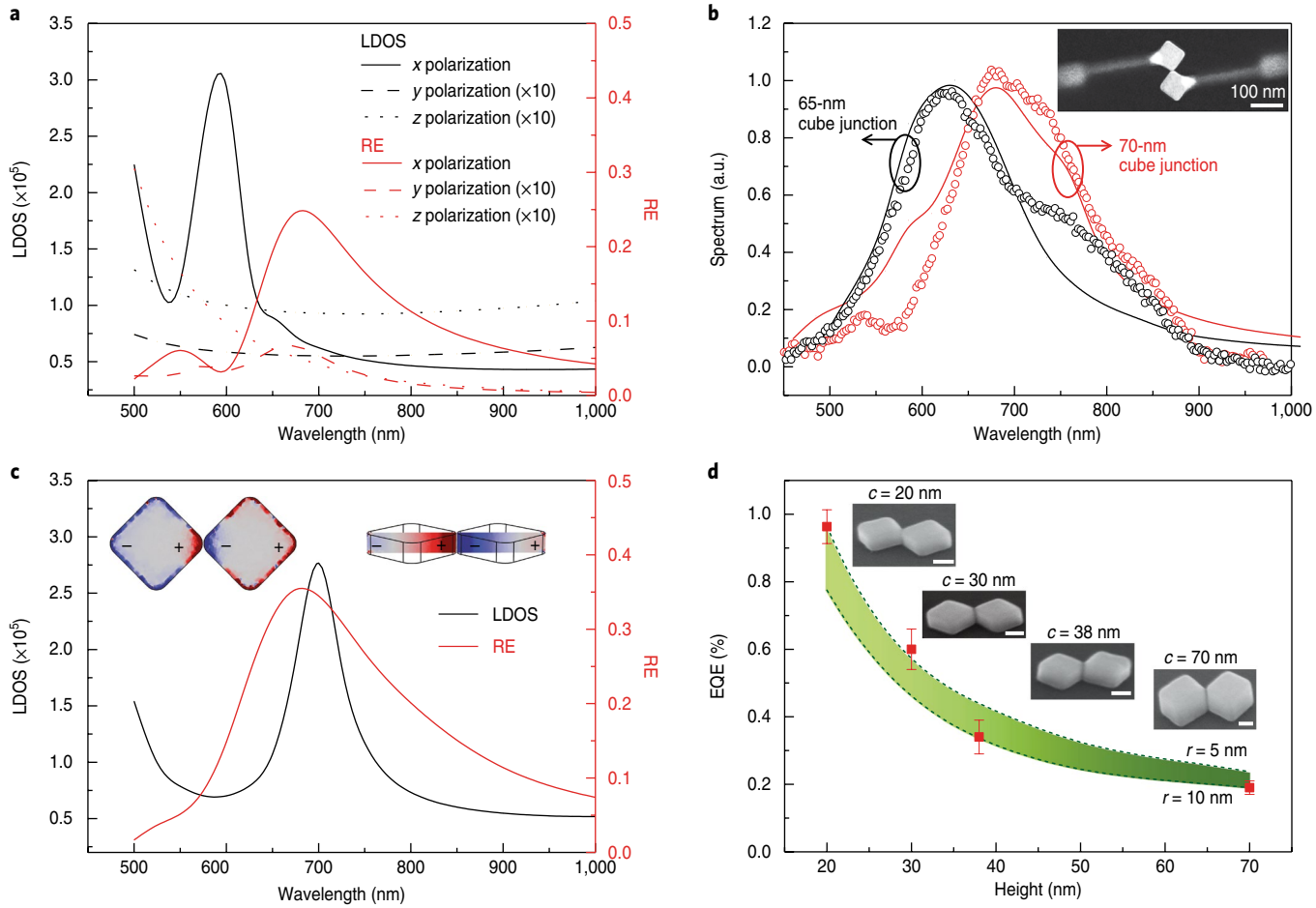

Fig. 2 | Investigation of Ag square-prism-based tunnel junctions. a, LDOS and radiation efficiency (RE) of Ag cubes (70 nm with edge curvature radius of 10 nm) for different polarizations of dipole located in the centre of the gap. **b**, Emission spectrum with 3.2 V applied across the tunnel junctions. The black and red circles represent measurement data for 65-nm and 70-nm cubes. The solid lines are simulation curves obtained by averaging *x*-polarized dipoles at multiple locations inside the gap (Supplementary Section 2). Inset, top-view scanning electron microscope (SEM) image of tunnel junction after Pt electrode deposition. **c**, LDOS and radiation efficiency of Ag square prisms with height $c = 20$ nm. The top insets show the charge distribution at the peak wavelength of the LDOS (700 nm). **d**, Experimental and simulated EQE of the tunnel junctions ($a = b = 70$ nm, $c = 20$ to 70 nm) (Supplementary Section 5). The green area represents the simulation results, with edge curvature radii *r* of 5 nm and 10 nm forming the upper and lower bounds. The red squares are the experimental results. The error bars represent the standard deviation obtained from measurements on multiple devices. The side-view SEM images placed near each point show samples used for the experiment. Scale bar, 40 nm.

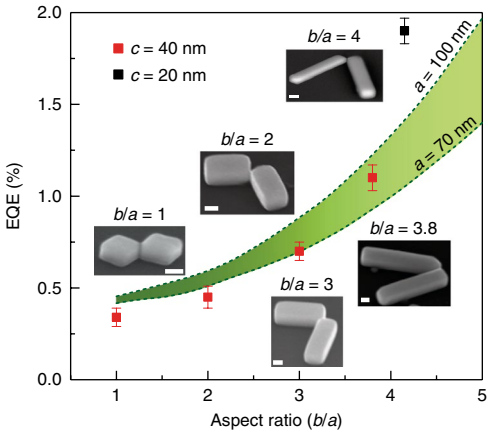

Fig. 3 | Numerical and experimental study of Ag nanobar-based tunnel junctions. Simulated and experimental EQE for various b/a ratios. The curved dashed lines that bound the green shaded area represent simulation results with planar width (a) of 70 nm and 100 nm. The red and black squares are the experimentally characterized results with $c = 40$ and $c = 20$, respectively. The error bars represent the standard deviation from measurements of multiple devices. The side-view SEM images placed near each point show samples used for the experiment. Scale bar, 40 nm.

stronger electron–plasmon interaction[1]. For a 1.5-nm gap, the plasmonic resonance is only slightly modified by considering either the nonlocal effect[17] or the quantum correlated model[18].

We started with electrical and optical characterization of a junction device formed by two 70-nm Ag nanocubes (Supplementary Sections 3 and 4). Using the applied voltage that corresponds to the maximum light emission, the emission spectrum of the nanojunction (red circles in Fig. 2b) shows a clear peak at ~680 nm, which agrees well with the simulation result (red solid curve in Fig. 2b). Once the light emission power has been obtained, the EQE (number of photons per electron) of the Ag-cube tunnel junctions can be calculated (Supplementary Section 5). This gives a result of $(1.8 \pm 0.2) \times 10^{-3}$ at the peak location of the light emission power, showing one order of magnitude improvement compared with previous work using an optical antenna[3,4].

One advantage of the metallic nanocrystal junction for light generation is the high tunability of the emission wavelength, which can be achieved by changing the size of the nanocrystal. To further confirm such scalability, a tunnel junction between 65-nm cubes was chosen. The corresponding emission spectrum measurement is again shown in Fig. 2b (black circles). As expected, the emission spectrum shifts to a shorter wavelength (peak ~625 nm). The EQE obtained for this tunnelling device is $(1.9 \pm 0.2) \times 10^{-3}$ (Supplementary Section 5), similar to that for the device using 70-nm cubes.

As can be seen from Fig. 2a, the peaks of the LDOS and of the radiation efficiency are misaligned, and this limits the light generation performance. The charge distribution of the nanocube junction at the peak wavelength of the LDOS is of high-order nature (Supplementary Section 6) rather than the simple dipole needed for maximum radiation efficiency, leading to the misalignment in the maxima. Further improvement in the performance of the device can be achieved by aligning the peaks of the LDOS mode and the radiation efficiency at the same emission wavelength, and this is demonstrated by shrinking the height of the cube to create a square prism. Figure 2c shows the simulated LDOS and radiation efficiency for a square-prism-based tunnel junction with height $c = 20$ nm (for more information, see Supplementary Section 6). The corresponding charge distribution at the peak wavelength of the LDOS is presented in the top inset of Fig. 2c, which confirms the dipole-mode oscillation. To fabricate the square-prism tunnel junction, we produced square-prism nanoparticles by a polyol synthesis process[19] and generated the nanojunction in a polystyrene matrix (Supplementary Section 1). Experimental characterization (Supplementary Section 4) shows that EQE is gradually improved by reducing the height of the square prisms, which agrees well with numerical predictions (see Fig. 2d). This optimization process improves the EQE of the nanojunction device to about 1%.

Another strategy for enhancing the EQE of the tunnel junction is to change the planar aspect ratio (b/a). The simulated LDOS and radiation efficiency of nanobar junctions with different b/a values are provided in Supplementary Sections 7–9. All of them show good alignment between LDOS and radiation efficiency peaks. With increasing b/a values, the LDOS gradually increases, and both LDOS and radiation efficiency peaks shift to longer wavelength with lower plasmonic loss, leading to improved EQE relative to a nanocube junction with $b/a = 1$. Experimental characterization (Supplementary Section 10) of nanobar junctions with different b/a values (red square in Fig. 3) shows increased EQE with higher b/a, which agrees with simulations (green shaded area in Fig. 3). The $b/a = 3.8$ nanobar junction shows an EQE of $(1.10 \pm 0.07) \times 10^{-2}$, which is 5.5 times as high as for the 70-nm nanocube junction. Note that the deviation between the experimental results and simulated predictions may result from the varied radius of curvature at the edge of the nanobar devices.

The EQE of tunnel junction can be further improved to ~2% (black square in Fig. 3) by using a junction between nanobars with $b/a = 4$ and $c = 20$ nm, combining the optimized height with the increasing b/a value of the nanobar. Figure 4a shows the measured light emission power detected at different voltages. The EQE of $(2.01 \pm 0.07) \times 10^{-2}$ is calculated by using the maximum emission power (Fig. 4b) at applied voltage ~1.5 V. The voltage-dependent light emission power is an interplay between the threshold voltage, the inelastic tunnelling current and the coupling between two electronic states, φ_1 and φ_2 (Supplementary Section 11). The emission spectrum shows maximum light generation at ~1,500 nm under an applied voltage of 1.5 V (black circles in Fig. 4b), which agrees well with the simulated prediction (solid line in Fig. 4b). Figure 4c shows that the emission is highly anisotropic and mainly dominated by x polarization (red circles), which agrees well with the simulation result (blue solid curve). The x-polarized emission pattern further verifies the dipole-mode emission from the Ag nanocrystal tunnel junctions.

Further enhancement of EQE may include reducing the gap distance between the nanocrystals in the tunnel junction and improving the shape of nanocrystal by using a smaller curvature radius at the corners. The theoretically predicted EQE of a nanobar tunnel junction with $c = 20$ nm can be enhanced to around 10% scale with an emission peak in the near-infrared region by using a corner curvature radius of 2 nm and a 1-nm gap (Supplementary Section 12). The performance could also be improved by low-temperature operation, because of the higher figure of merit ($|\varepsilon' / \varepsilon''|$, the magnitude of the ratio of the real to the imaginary part of the permittivity) of the plasmonic material[15] and improved thermal stability. Another direction for future exploration could be to improve the inelastic tunnelling current by designing resonant tunnel junctions[20–22].

In conclusion, light generation through inelastic electron tunnelling has been explored in Ag tunnel junction structures with various geometries. The combination of the high radiation efficiency of edge-to-edge assembled single-crystalline Ag nanoantenna with a large LDOS in the ultra-small tunnelling gap greatly increases the far-field light emission efficiency from spontaneous inelastic tunnelling to ~2%. Other than the methods mentioned above, the emission efficiency could be further improved by directly coupling the radiation to on-chip components such as waveguides or cavities, so

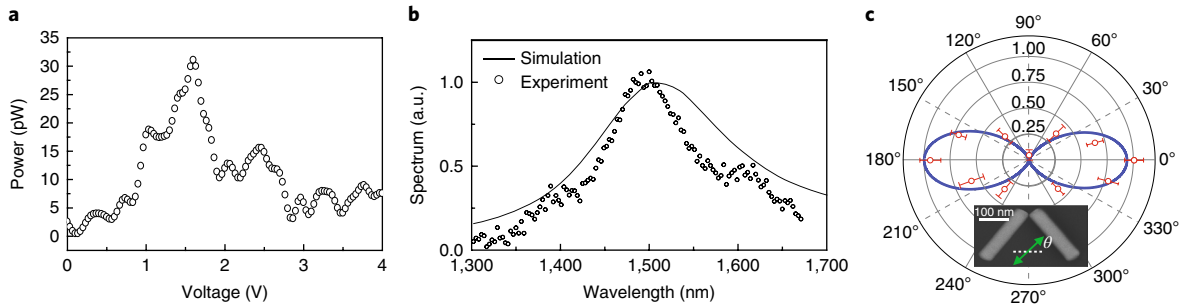

Fig. 4 | Silver nanobar-based tunnel junction with optimized EQE. a, Experimental characterization of the emission power at different voltages. **b**, Emission spectrum measured at an applied voltage of 1.5 V. **c**, Emission polarization from both simulation (blue line) and experimental measurement (red circles). The error bars represent the standard deviation from measurement results of multiple devices. The simulation is done by placing a dipole with *x*, *y* or *z* polarization in the centre of the gap, and taking the far-field radiation result. The angle corresponds to θ as marked in the top view of a Ag nanobar junction with size (280×65×20) nm. The white dashed line represents the device direction and the green arrow the direction of the detection polarizer.

that the device could be integrated into photonics and/or plasmonic systems for on-chip applications[23–26]. In principle, the emission frequency of the MIM junction device could cover a range from ultraviolet to mid-infrared, although the details of the material and junction configurations need to be designed accordingly. Optical interconnections using light-emitting sources based on tunnel junctions will make it possible to achieve an extremely large bandwidth for greatly improved speed and quality of communications.

Methods

Methods, including statements of data availability and any associated accession codes and references, are available at https://doi.org/10.1038/s41566-018-0216-2.

Received: 19 November 2017; Accepted: 20 June 2018;
Published online: 23 July 2018

References

1. Lambe, J. & McCarthy, S. L. Light emission from inelastic electron tunneling. *Phys. Rev. Lett.* **37**, 923–925 (1976).
2. Davis, L. C. Theory of surface-plasmon excitation in metal–insulator–metal tunnel junctions. *Phys. Rev. B* **16**, 2482–2490 (1977).
3. Kern, J. et al. Electrically driven optical antennas. *Nat. Photon.* **9**, 582–586 (2015).
4. Parzefall, M. et al. Antenna-coupled photon emission from hexagonal boron nitride tunnel junctions. *Nat. Nanotech.* **10**, 1058–1063 (2015).
5. Persson, B. N. J. & Baratoff, A. Theory of photon-emission in electron-tunneling to metallic particles. *Phys. Rev. Lett.* **68**, 3224–3227 (1992).
6. Ranuárez, J. C., Deen, M. J. & Chen, C.-H. A review of gate tunneling current in MOS devices. *Microelectron. Reliab.* **46**, 1939–1956 (2006).
7. McCarthy, S. L. & Lambe, J. Enhancement of light emission from metal–insulator–metal tunnel junctions. *Appl. Phys. Lett.* **30**, 427–429 (1977).
8. Kirtley, J., Theis, T. N. & Tsang, J. C. Light-emission from tunnel-junctions on gratings. *Phys. Rev. B* **24**, 5650–5663 (1981).
9. Berndt, R., Gimzewski, J. K. & Johansson, P. Inelastic tunneling excitation of tip-induced plasmon modes on noble-metal surfaces. *Phys. Rev. Lett.* **67**, 3796–3799 (1991).
10. Sparks, P. D., Sjodin, T., Reed, B. W. & Stege, J. Light-emission from the slow mode of tunnel-junctions on short-period diffraction gratings. *Phys. Rev. Lett.* **68**, 2668–2671 (1992).
11. Junichi, W., Yoichi, U., Junichi, M. & Sukekatsu, U. Light emission from Si-metal–oxide–semiconductor tunnel junctions. *Jpn. J. Appl. Phys.* **32**, 99 (1993).
12. Siu, D. P., Jain, R. K. & Gustafson, T. K. Stimulated electron tunneling in metal–barrier–metal structures due to surface plasmons. *Appl. Phys. Lett.* **28**, 407–410 (1976).
13. Novotny, L. & van Hulst, N. Antennas for light. *Nat. Photon.* **5**, 83–90 (2011).
14. Bharadwaj, P., Deutsch, B. & Novotny, L. Optical antennas. *Adv. Opt. Photonics* **1**, 438–483 (2009).
15. Jayanti, S. V. et al. Low-temperature enhancement of plasmonic performance in silver films. *Opt. Mater. Express* **5**, 1147–1155 (2015).
16. Gao, B., Arya, G. & Tao, A. R. Self-orienting nanocubes for the assembly of plasmonic nanojunctions. *Nat. Nanotech.* **7**, 433–437 (2012).
17. García de Abajo, F. J. Nonlocal effects in the plasmons of strongly interacting nanoparticles, dimers, and waveguides. *J. Phys. Chem. C.* **112**, 17983–17987 (2008).
18. Esteban, R., Borisov, A. G., Nordlander, P. & Aizpurua, J. Bridging quantum and classical plasmonics with a quantum-corrected model. *Nat. Commun.* **3**, 825 (2012).
19. Hsu, S.-W. & Tao, A. R. Halide-directed synthesis of square prismatic Ag nanocrystals by the polyol method. *Chem. Mater.* (in the press); https://doi.org/10.1021/acs.chemmater.8b01166.
20. Uskov, A. V. et al. Excitation of plasmonic nanoantennas by nonresonant and resonant electron tunnelling. *Nanoscale* **8**, 14573–14579 (2016).
21. Capasso, F., Mohammed, K. & Cho, A. Resonant tunneling through double barriers, perpendicular quantum transport phenomena in superlattices, and their device applications. *IEEE J. Quantum Electron.* **22**, 1853–1869 (1986).
22. Braginskiĭ, L. S. & Baskin, É. M. Inelastic resonant tunneling. *Phys. Solid State* **40**, 1051–1055 (1998).
23. Schubert, E. F. & Kim, J. K. Solid-state light sources getting smart. *Science* **308**, 1274–1278 (2005).
24. Du, W., Wang, T., Chu, H.-S. & Nijhuis, C. A. Highly efficient on-chip direct electronic–plasmonic transducers. *Nat. Photon.* **11**, 623–627 (2017).
25. Fang, Y. & Sun, M. Nanoplasmonic waveguides: towards applications in integrated nanophotonic circuits. *Light Sci. Appl.* **4**, e294 (2015).
26. de Vega, S. & García de Abajo, F. J. Plasmon generation through electron tunneling in graphene. *ACS Photonics* **4**, 2367–2375 (2017).
27. Rawat, A. et al. Optical band gap of polyvinylpyrrolidone/polyacrilamide blend thin films. *Indian J. Pure Appl. Phys.* **50**, 100–104 (2012).

Acknowledgements

This work is financially supported by the Defense Advanced Research Projects Agency (DARPA) Microsystems Technology Office (W911NF-16-2-0156). We thank J. Conway for suggestions.

Author contributions

Z.L. conceived the project. H.Q. and S.-W.H. designed the structures. H.Q. performed the experiments. S.-W.H. and K.G. prepared and characterized the Ag nanocrystals. H.Q. performed the theoretical work. H.Q., S.-W.H., K.G., C.T.R., J.Z., D.L., A.R.T. and Z.L. wrote the manuscript. All authors analysed the data and contributed to the discussion. A.R.T. and Z.L. supervised the research.

Competing interests

The authors declare no competing interests.

Additional information

Supplementary information is available for this paper at https://doi.org/10.1038/s41566-018-0216-2.

Reprints and permissions information is available at www.nature.com/reprints.

Correspondence and requests for materials should be addressed to A.R.T. or Z.L.

Publisher's note: Springer Nature remains neutral with regard to jurisdictional claims in published maps and institutional affiliations.

Methods

Numerical simulation. Numerical finite-element simulations were performed with COMSOL Multiphysics software. The LDOS and radiation efficiency were simulated by placing a dipole in the tunnelling junction gap, with the Ag material property taken from ref. [28] and polyvinylpyrrolidone (PVP) from ref. [29]. The unit for the LDOS is the DOS of vacuum.

Sample preparation. Details of the fabrication of the Ag nanoparticle-based tunnel junction are provided in Supplementary Section 1. The electrode of the tunnel junction device is produced by focused-ion-beam assisted Pt deposition. The connection area between the cubes and electrodes is milled by the ion beam to remove the polymer before Pt deposition.

Sample characterization. Details of the measurement set-up for the inelastic tunnel devices are provided in Supplementary Section 3.

Data Availability. The data that support the plots within this paper and other findings of this study are available from the corresponding author upon reasonable request.

References

28. Palik, E. D. *Handbook of Optical Constants of Solids* (Academic, San Diego, CA, 1998).
29. König, T. A. F. et al. Electrically tunable plasmonic behavior of nanocube–polymer nanomaterials induced by a redox-active electrochromic polymer. *ACS Nano* **8**, 6182–6192 (2014).